



UNIVERSITÀ  
DEGLI STUDI  
FIRENZE

# FLORE

## Repository istituzionale dell'Università degli Studi di Firenze

### **Static and dynamic experimental validation of analytical homogenization models for corrugated core sandwich panels**

Questa è la Versione finale referata (Post print/Accepted manuscript) della seguente pubblicazione:

*Original Citation:*

Static and dynamic experimental validation of analytical homogenization models for corrugated core sandwich panels / Bartolozzi G.; Baldanzini N.; Pierini M.; Zonfrillo G.. - In: COMPOSITE STRUCTURES. - ISSN 0263-8223. - ELETTRONICO. - 125:(2015), pp. 343-353. [10.1016/j.compstruct.2015.02.014]

*Availability:*

The webpage <https://hdl.handle.net/2158/995606> of the repository was last updated on 2021-03-30T14:19:58Z

*Published version:*

DOI: 10.1016/j.compstruct.2015.02.014

*Terms of use:*

Open Access

La pubblicazione è resa disponibile sotto le norme e i termini della licenza di deposito, secondo quanto stabilito dalla Policy per l'accesso aperto dell'Università degli Studi di Firenze (<https://www.sba.unifi.it/upload/policy-oa-2016-1.pdf>)

*Publisher copyright claim:*

Conformità alle politiche dell'editore / Compliance to publisher's policies

Questa versione della pubblicazione è conforme a quanto richiesto dalle politiche dell'editore in materia di copyright.

This version of the publication conforms to the publisher's copyright policies.

La data sopra indicata si riferisce all'ultimo aggiornamento della scheda del Repository FloRe - The above-mentioned date refers to the last update of the record in the Institutional Repository FloRe

(Article begins on next page)

# Static and dynamic experimental validation of analytical homogenization models for corrugated core sandwich panels.

Giorgio Bartolozzi<sup>a,\*</sup>, Marco Pierini<sup>a</sup>, Niccolò Baldanzini<sup>a</sup>, Giovanni Zonfrillo<sup>a</sup>

<sup>a</sup>*Dipartimento di Ingegneria Industriale, Università degli Studi di Firenze, Via di Santa Marta 3, 50139 Firenze, Italy*

---

## Abstract

A typical procedure to speed up simulations involving corrugated core sandwich panels consists in replacing the complex shaped core with an equivalent homogeneous layer. The properties of the equivalent material, usually orthotropic, can be determined by means of FE-based techniques, experimental tests or analytical formulations. In particular, analytical methodologies have been deeply investigated in the last decades in the literature, leading to a general formulation valid for every kind of corrugations.

The aim of this paper is to perform an experimental campaign on some available sinusoidal corrugated core panels. Moreover, the mentioned general formulation is extended and it is used to build homogenized models. An investigation is carried out on the deviation of the corrugation from the idealized sinusoidal shape and its effects on equivalent parameters. Results from the measurements, in terms of static and dynamic behaviour, will be compared to numerical data obtained from the homogenized models, assuming either an idealized sinusoid or the real corrugation. The importance of accurately representing the core shape is proved by the greater accuracy provided by the general formulation.

## Keywords:

Sandwich structures, Corrugated core, Homogenized models, Experimental validation

---

\*Corresponding author. Tel.: +39 055 4796487; fax: +39 055 4796489.  
Email address: [g.bartolozzi@unifi.it](mailto:g.bartolozzi@unifi.it) (Giorgio Bartolozzi)

---

## 1. Introduction

Corrugated core sandwich structures are increasingly being used in several industrial areas, as they provide good structural, acoustic and thermal properties with limited weight. The main applications are in the transportation industry which is looking at innovative multi-functional components as the sandwich structures may be. Among the several investigated properties, the high stiffness-to-mass ratio, especially in bending condition, is mainly influenced by the two faces of the sandwich structure. Nevertheless other properties, such as acoustic or thermal insulation, are governed by the core. Therefore, increasing interest is focused on the modelling of the core behaviour. In particular, in order to speed up simulations and have reliable and accurate prediction tools, usually the homogenization of the core is carried out, which consists in replacing the heterogeneous core layer with an equivalent material model. In this context, among the several analytical formulations available in the literature for the different corrugation profiles, the authors developed in a previous work [1] a general analytical formulation which is valid for every corrugated core shape. The accuracy of the formulation in predicting the equivalent mechanical parameters for the core was proved by means of FE simulations. Nevertheless, FE models are typically built modelling the structures based on some, even strict, hypotheses. Therefore, to prove the modelling to be representative of the real sandwich structure behaviour, an experimental campaign is needed.

Several researches are reported in the literature aiming at testing sandwich structures, but very few are available for corrugated core panels, which are the subject of this paper. Carlsson et al. [2] determined the in-plane and out-of-plane shear stiffness together with the bending rigidity of corrugated cardboard. The bending properties were experimentally determined also by Gilchrist et al. [3]. Still on cardboard panels, there is a series of tests by Aboura, Allaoui et al. [4, 5, 6] to determine their tensile properties and the failure phenomena. Other studies concerning cardboard panels investigated the buckling behaviour in the in-plane directions, e.g [7, 8], and in the through-thickness direction, e.g. [9]. Finally, also testing of the performance under impact conditions is found in the literature, e.g. [10].

Moving to all-metal corrugated sandwich panels, very few papers are found in the literature dealing with experimental testing. Among them, it

Panel denomination	Thickness face 1 [mm]	Core sheet thickness [mm]	Thickness face 2 [mm]	Total height [mm]	Period [mm]
05_02_05 H6	0.5	0.2	0.5	6.0	2.50
08_02_05 H6	0.8	0.2	0.5	6.0	4.24
10_03_10 H6	1.0	0.3	1.0	6.0	4.25
10_03_10 H11.5	1.0	0.3	1.0	11.5	7.14

Table 1: Main dimensions of the available panels.

is worth citing the work by Knox et al. [11] on steel trapezoidal corrugated panels and that by Magnucki et al. [12] on aluminum sinusoidal corrugated panels. Both papers mainly focus on the bending rigidity of these structures, since it is one of the most important characteristics. In particular, the work by Magnucki et al. [12] investigated the same panels which are the subject of the present paper, i.e. sandwich panels with sinusoidal corrugated core.

The aim of this paper is to analyse and assess the precision and accuracy of the analytical modelling developed in [1] versus a measurement campaign, which involved both the static and dynamic behaviour of the sandwich structure. The importance of using a general formulation as the one given in [1], which is able to represent every corrugation profile by means of a Fourier series representation, is assessed comparing it with a specific formulation for perfect sinusoidal shapes.

Four different panels are available for the present work, whose main characteristics are listed in Table 1. Within the selected set of panels, the geometric features of the sinusoidal corrugation, i.e. amplitude and period, vary significantly. These dimensions are fundamental to determine the equivalent properties of the core and therefore to determine the overall behaviour of the sandwich panel. Typically, the amplitude of the sine curve is supposed to be half the core height, thus excluding the thickness of the corrugated lamina which is usually considered negligible, while the period must be measured and is reported in the last column of Table 1.

This paper is organized as follows. In Section 2, an extension of the general formulation given in [1] is proposed. In Section 3, the influence of manufacturing processes on the real corrugation profiles is investigated and discussed. Section 4 presents the experimental campaign setup both for the determination of modal characteristics and tensile properties. Finally, in Section 5 results from the measurements are presented, compared with homogenized models and discussed.

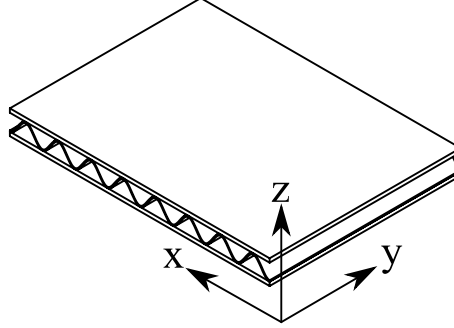


Figure 1: Global system of reference definition.

## 2. Additional parameters for the analytical modelling

Before going into details about the measurement campaign, it is worth highlighting a peculiarity of the analytical formulation developed by the authors in [1]. It was noted by the authors that, while determining the in-plane shear modulus, the values of  $G_{xy}$  and  $G_{yx}$  – determined in pure shear conditions – were not equivalent. The same behaviour has been observed later while determining the shear moduli in the other two planes, i.e.  $xz$  and  $yz$  – see Figure 1 for the reference system.

Nevertheless, the FE models used in the following require a unique value for the orthotropic material definition. Therefore, it is important to specify which parameters are used in the following modelling. For the  $xz$ - and  $yz$ -plane,  $G_{zx}$  and  $G_{zy}$  are used respectively, since in the notation used – see [1] for more details on the convention – these parameters are computed by deriving the displacements in the  $z$ -direction, which is the direction where vibrations are measured by the accelerometers. Consequently, the  $G_{yx}$  parameter is chosen for the  $xy$ -plane to maintain accordance with subscript notation. In the following the parameters  $G_{zx}$  and  $G_{zy}$  are derived, since they were not reported in the previous work.

### 2.1. Transverse shear modulus in $xz$ -plane $G_{zx}$

The procedure is similar to what already shown in [1], which is based on a Fourier's series representation of the corrugation. In particular, the corrugation is allowed to be also asymmetric, and the corrugation is therefore subdivided in two parts as in [1], with half-period  $p_1$  and  $p_2$ , as in Figure 2. According to the convention used, the  $G_{zx}$  parameter is computed applying

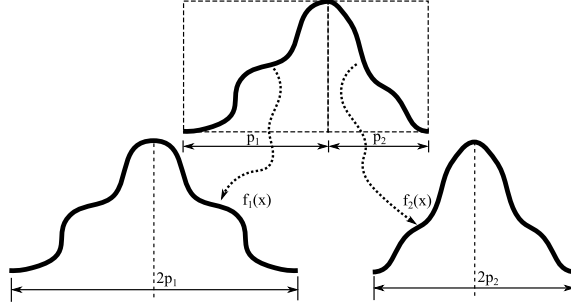


Figure 2: Mirroring process to obtain the two parts of the corrugation.

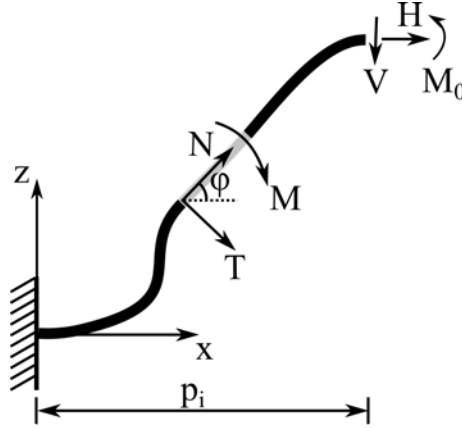


Figure 3: Loads and forces acting on the centre line of the corrugation: nomenclature.

at the upper end of the two parts of the corrugation a force  $V$  along the  $z$ -direction and determining the displacement in the same direction. Referring to Figure 3, which considers a unit width specimen and it is valid for each of the two parts, other displacements and rotations of the upper edge are denied, while the lower edge is fully clamped – please note that the periodic nature of the corrugation is implicitly considered by the imposed BCs.

With reference to Figure 3, the vertical force  $V$  is imposed to be unitary, while a dummy force  $H$  and dummy moment  $M_0$  are included to impose the mentioned BCs, i.e. horizontal displacement  $\delta_H$  and rotation  $\delta_{M_0}$  of the upper edge equal to zero.

The same system of equations as in [1] can be obtained by imposing the Castigliano's theorem [13],

$$\begin{bmatrix} \delta_{H_i} \\ \delta_{V_i} \\ \delta_{M_{0i}} \end{bmatrix} = \frac{1}{EA} \begin{bmatrix} C_{1,1} & C_{1,2} & C_{1,3} \\ & C_{2,2} & C_{2,3} \\ sym. & & C_{3,3} \end{bmatrix} \begin{bmatrix} H \\ V \\ M_0 \end{bmatrix} \quad (1)$$

being  $E$  the Young's modulus of the constituent material of the corrugation and  $A$  the area of the corrugated lamina cross-section. The reader is referred to [1] for the complete explanation of the terms  $C_{i,j}$ .

The vertical displacement can then be computed for each of the two parts as

$$\delta_{V_i} = \frac{1}{EA} \frac{\det(C)}{\det(C_{red}^1)} \quad (2)$$

where  $C_{red}^1$  is defined as follows:

$$[C_{red}^1] = \begin{bmatrix} C_{1,1} & C_{1,3} \\ C_{3,1} & C_{3,3} \end{bmatrix} \quad (3)$$

The total shear behaviour of a complete corrugation period  $P_0$  can be seen as the combination of the two parts, which behave as two springs in series. Therefore, once the vertical displacement for the two parts,  $\delta_{V_1}$  and  $\delta_{V_2}$  respectively, are calculated at the free edge, the total displacement  $\delta_V$  is found as the sum of those values. Finally, the shear modulus  $G_{zx}$  of the equivalent material is

$$G_{zx} = \frac{\tau_{zx}}{\gamma_{zx}} = \frac{F_z}{A_{zy}} \bigg/ \frac{\delta_z}{l_x} = \frac{P_0}{H_0} \cdot \frac{1}{\delta_V} \quad (4)$$

where  $H_0$  is the corrugation height – the reader is referred to [1] to completely understand the middle passage.

As already explained in [1], in order to have a parameter representative of a plate situation rather than a beam structure, the Young's modulus in Eq. 2 should be replaced by the plate modulus  $E/(1 - \nu^2)$ .

## 2.2. Transverse shear modulus in $yz$ -plane $G_{zy}$

The  $G_{zy}$  parameter can be found applying a force  $V$  along  $z$  in the  $xz$ -plane and calculating the deriving displacement. The procedure used is similar to the one shown for  $G_{xy}$  in [1]. The same relations can be found as for the  $G_{xy}$  parameter under the same assumptions and the following relation is determined:

$$G_{zy} = G_{xy} \quad (5)$$

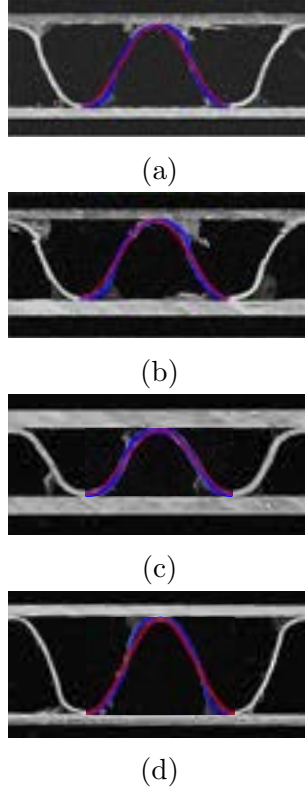


Figure 4: Comparison of theoretical sine (red lines) and real curves (blue lines) on the scanned images.

### 3. Real shape influence

When observing the cross sections of the panels, it is evident that the real shape of the corrugation differs from the theoretical sinusoidal profile. In Figure 4, the comparison between sinusoidal and real shape is shown. As visible in the figure, the real corrugation shows also a strongly non-symmetric profile. Therefore, in order to compute the parameters for the equivalent material, it is necessary to use the general formulation proposed in [1] and not the specific formulation developed for sinusoidal corrugations by the authors in [14]. To represent the real shapes with sufficient accuracy, the expression in Fourier series used in [1] is extended to all terms whose coefficient is greater than  $10^{-6}$ . As an example, to represent each of the two parts of the core profile of the “10\_03\_10 H11.5” panel – see Table 1 and Figure 4a –, the first 34 series terms are needed.



Case	$E_x$ [MPa]	$E_y$ [MPa]	$\nu_{xy}$ [-]	$G_{yx}$ [MPa]	$G_{zx}$ [MPa]	$G_{zy}$ [MPa]
05_02.05 H6 – Alu 5182-H48						
Sinusoidal	2.757	4.351E+3	2.091E-4	6.697E+2	2.493E+2	1.636E+3
Real	2.326	4.570E+3	1.680E-4	6.376E+2	8.185E+1	1.718E+3
Difference [%]	-15.6	+5.03	-19.7	-4.79	-67.2	+5.01
08_02.05 H6 – Alu 5754-H48						
Sinusoidal	3.450	4.517E+3	2.520E-4	7.447E+2	2.721E+2	1.698E+3
Real	2.972	4.723E+3	2.077E-4	7.124E+2	9.006E+1	1.775E+3
Difference [%]	-13.9	+4.56	-17.6	-4.34	-66.9	+4.53
10_03.10 H6 – Alu 5754-H48						
Sinusoidal	21.44	7.221E+3	9.800E-4	1.447E+3	8.252E+2	2.715E+3
Real	18.33	7.490E+3	8.076E-4	1.395E+3	3.946E+2	2.816E+3
Difference [%]	-14.5	+3.73	-17.6	-3.59	-52.2	+3.72
10_03.10 H11.5 – Alu 5754-H48						
Sinusoidal	1.276	3.752E+3	1.122E-4	4.938E+2	1.611E+2	1.411E+3
Real	1.094	3.926E+3	9.191E-5	4.719E+2	5.259E+1	1.476E+3
Difference [%]	-14.3	+4.64	-18.1	-4.43	-67.4	+4.61

Table 2: Comparison of core equivalent parameters for theoretical and real corrugation profiles.

Material	Young's modulus [MPa]	Poisson's ratio [ad.]	Density [kg/m <sup>3</sup> ]
Alu 5754-H48	70300	0.33	2670
Alu 5182-H48	69600	0.33	2670

Table 3: Aluminum properties used.

To have an idea of the influence of the real corrugation shape on the equivalent parameters, values obtained assuming the theoretical sinusoidal shape are compared to those supposing the real corrugation. Results of this comparison are shown in Table 2. Please note that a plate representation is assumed and only one shear modulus for each plane is considered. To obtain the real geometry of the corrugation, a scan of the cross section of the panels were made and the image obtained were processed to obtain the midplane curve (Figure 4). Two different constituent materials were considered for the corrugated laminas according to manufacturer's datasheets. The properties of such materials are given in Table 3.

It is evident from Table 2 that the most relevant differences are on  $E_x$

and  $G_{zx}$  which are likely to have a strong influence both on the static and the dynamic behaviour of the structure. In particular, the real shape implies a reduction of about 60% in the  $G_{zx}$  parameter and a reduction of about 14% on the  $E_x$  parameter. The changes on the other moduli are mainly due to the different length of the corrugation and vary in the range  $\pm 4/5\%$ .

It is then obvious that, in order to properly reproduce the behaviour of the real panels, it is important to build the FE equivalent models using the parameters shown in Table 2 for the real shape.

## 4. Experimental methodology

### 4.1. Modal analysis

Modal analysis can be defined as the study of the dynamic characteristics of a mechanical structure. The comparison of predicted structural dynamic behaviour with experimentally measured data is fundamental in validating the modelling of a complex structure as the sandwich panels investigated here. Indeed, if the influence of the core can be usually neglected in static bending conditions, the elastic moduli of the core have a strong influence on mode shapes and frequencies. Moreover, since the developed analytical formulation for the homogenization of the core is based on a static equivalence, it is interesting to investigate the accuracy in reproducing the dynamic behaviour of the structures.

#### 4.1.1. Methodology

Thanks to the light damping of the structure, an impact testing can be considered a good methodology to obtain the modal characteristics of the panel. The specimen has been subjected to impulses through a hard tipped hammer, Bruel & Kjaer type 8202. The Impact Hammer Type 8202 is an instrumented hammer provided with a built-in Force Transducer Type 8200 with a sensitivity of 0.98 pC/N. The response has been measured through four piezoelectric uniaxial accelerometers. In particular:

- 2 PCB Model 352C22;
- 2 ENDEVCO Model 2250AM1-10.

The sensitivity of the accelerometers is 10 mV/g (1.0 mV/(m/s<sup>2</sup>)) and the mass is approximately 0.5 g. The impulse and the responses are acquired

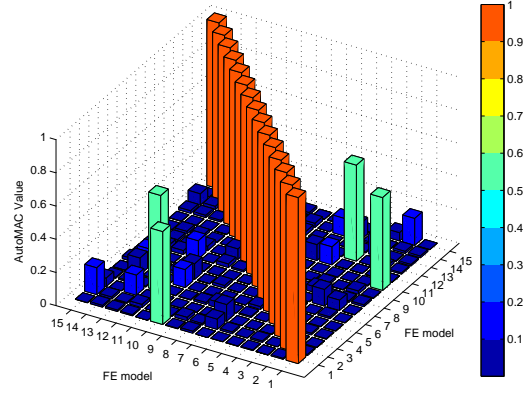


Figure 5: AutoMAC matrix for measurement point selection.

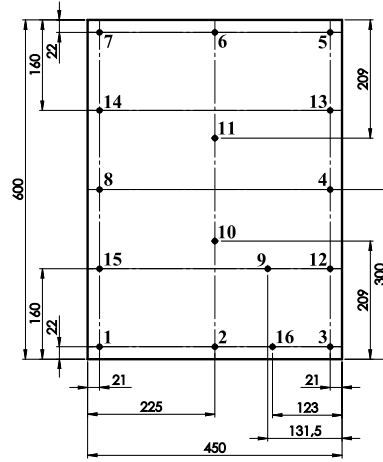


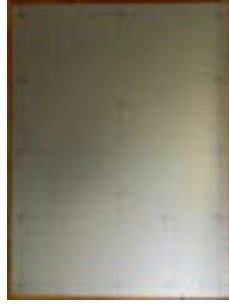
Figure 6: Positions of stations for the modal testing.

with an LMS SCADAS III SC-310 acquisition system and data are pre- and post-processed with LMS Test.Lab.

A roving hammer technique is used. The choice of the excitation stations was made by a preprocessing of the FEM models, specifically computing the AutoMAC of the structure to check if the mode shapes defined at the chosen DOFs well represent the mode shapes of the complete FEM model, see [15] and Section 5.1 for a deeper explanation of the correlation method used. The first 15 modes were considered. In Figure 5 it is shown an example of the results obtained for the set of 16 stations chosen. In Figure 6, a scheme with the selected points for the acquisition is shown. Nevertheless, given the rather simple overall geometry of the panel, i.e. a rectangle, the modal testing is more focused on determining the eigenfrequencies, rather than the eigenmodes of the structure. Finally, the measurement stations were identified by using the Driving Point Residues (DPR): this technique allows determining the more influent points for a given set of modes. The response has been measured by placing the accelerometers at stations 5, 10, 14 and 16 – see Figure 6 for point identification. FRFs are computed between each impact DOF and the fixed response DOFs. In order to reduce the statistical variance of a measurement, an averaging process was implemented by repeating 5 times each acquisition. Finally, the estimation of the modal parameters is done by using the LMS PolyMAX tool.

#### *4.1.2. Specimen details*

The four panels have an overall dimension of  $450 \times 600$  mm. Each of them was marked in order to easily identify the excitation points, Figure 7a. Measurement stations were chosen on the opposite side of the panel, see Figure 7b. Free boundary conditions for the modal testing was chosen. The free condition would mean that the structure is, in effect, floating in space with no attachments to ground and exhibits rigid body behaviour at zero frequency. Physically, this is not realizable, so the structure was suspended as depicted in Figure 8, using a very soft spring. By doing this, the structure will be constrained to a degree and the rigid body modes will no longer have zero frequency. However, if a sufficiently soft support system is used, the rigid body frequencies will be much lower than the frequencies of the flexible modes and thus have negligible effect. The rule of thumb for free supports is that the highest rigid body mode frequency must be less than one tenth that of the first flexible mode. If this criterion is met, rigid body modes will have negligible effect on flexible modes. In order to modify as less as possible the



(a)



(b)

Figure 7: Panel marked and equipped: (a) Front face – excitation points, (b) Rear face – measurement points.

panel, and consequently its dynamic characteristics, the connection with the springs is done by inserting a very light string in a small hole close to the edge of the panel.

#### 4.1.3. *FE models*

The FE models to be validated are built using a multi-layer description in Nastran [16] by means of the PCOMP card, which allows defining layers of different material, thickness and/or orientation. This information is then used by the software to compute, assuming perfect bonding between layers, an equivalent shell property. Three layers are considered to represent the two skins and the equivalent layer for the core. The FE mesh is properly built to have nodes in correspondence of the measurement points of the panel. The first 15 modes are then computed by the standard Lanczos method.

An important note must be done on the equivalent core material. Equivalent properties are derived as in [1], apart for the out-of-plane shear moduli.



Figure 8: Support of the panel for modal testing.

It has been shown in Section 2 which parameters are used.

Finally, since the total mass is a very important parameter on the values of the natural frequencies, a non structural mass is added to the FE models in order to meet the measured mass of the tested panels, which varies between 1.0 and 1.9 kg depending on the panel configuraon. Typically, this difference in the total mass is between 0.1 and 0.2 kg and it can be mainly attributed to the presence of the glue, which is not accounted for in the modelling, but has a non-negligible mass.

#### 4.2. Tensile testing

Testing of average (homogenized) mechanical properties for the sole corrugated core is a very difficult task. The typical properties which are usually “directly” measured are the tension and compression characteristics in the through-thickness direction according to ASTM C297 [17] and ASTM C365 [18] respectively. Moreover, the out-of-plane shear moduli can be determined following test procedure in ASTM C273 [19]. Nevertheless, even for such cases, they are not real *direct* measurements, since the core must be adhesively bonded to two steel blocks which reproduce the coupling and constraint of the core from the skins of the sandwich panel.

Moving to the in-plane properties, typically testing is performed on the complete sandwich structure, even though some example on small corrugated composite lamina exists in the literature, e.g. the tensile test in [20]. Even more often, for tensile testing in the in-plane directions, only face sheets are considered, since these elements give the main contribution to the total

stiffness. This is true for particularly weak cores, but cannot be stated a priori on all-metal corrugated sandwich structures.

In this section, the tensile testing performed on the sinusoidal corrugated core sandwich panels available is presented and discussed. Please note that the analytical values of the total panel were obtained from those of the different layers by using relations from the classical lamination theory. In particular, equivalent core Young's moduli, i.e.  $E_x$  and  $E_y$ , for the core are taken as in [1].

#### 4.2.1. Methodology

The tensile testing was performed on a servohydraulic testing system, the *MTS810 Material Test System*. The force applied by the machine to the specimen ranges from 25 kN to 500 kN. Nevertheless, due to an amplification factor, for these tests, the full scale value was chosen to be 50 kN. The tests were performed with a displacement-controlled technique and the velocity was approximately 0.067 mm/s. The acquisition was made with a frequency of 20 Hz, thus data were acquired every 0.05 seconds. The value of the applied force was measured from the load cell, while strain was measured by a static strain gauge extensometer (*MTS 632.11F-20*) with a full scale displacement of 3.75 mm. The acquisition was controlled by the control unit *MTS 458.20 Micro Console*. In Figure 9 an example is shown of mounted and instrumented specimens for tensile testing in both  $x$ - and  $y$ -directions.

Tests were performed until fracture happened. Nevertheless, the extensometer was removed after a certain displacement was reached (approximately 2.5 mm). Indeed, since the purpose of the tensile testing is to compare the equivalent Young's modulus, only the initial part of the test is needed, i.e. the elastic part. Finally, for each panel, the test was carried out on 5 specimens to account for uncertainties and statistical variance of the measurements – see Figure 10 for a view of some specimens.

#### 4.2.2. Specimen details

There is no specific standard which rules the tensile testing for metallic sandwich panels. Therefore, according to the standard ASTM E8 [21], which is valid for tensile testing of metallic materials, the specimen for these panels should have a reduced cross-section in the gage area, relative to that of the remainder of the specimen, so that deformation and failure will be localized in this region. Nevertheless, the presence of the corrugation makes



(a)



(b)

Figure 9: Tensile test setup for testing along the: (a) *y-direction*, (b) *x-direction*.





Figure 10: Tensile test specimens.



Figure 11: Resin reinforced specimens.

the preparation of such a specimen very difficult. Moreover, in the transition area, the corrugated core would be cut in diagonal, so that the forces could be improperly transferred in the core from the grip section to the gage area. For these reasons, in the present test campaign, rectangular specimens are chosen. For this kind of specimens, sometimes it is required the use of tabs in the gripping area with a bevel to ensure a successful introduction of the load into the specimen and the prevention of premature failure due to a significant discontinuity. Nevertheless, ASTM D3039 [22] specifies that the introduction of tabs, either friction or bonded type, is not always required and it suggests to evaluate the need to use tabs by the end results. In this regard, in the present experimental activity, some preliminary tests were carried out to check an acceptable failure location. Therefore, the specimen created has the following dimensions: length of 200 mm in the tensile direction and approximately 25 mm width. The width varies from panel to panel, because specimens for testing in the *y-direction* are built to include a finite number of corrugation periods in their width: 3 periods for the 6 mm thick panels and 2 periods for the 11.5 mm thick panel.

Since the panel is subjected to strong compression in the gripping areas, the core may be crushed in that area, resulting in possible slips and ineffective testing. To avoid this phenomenon, wedge action grips were used and the core corrugations in the gripping area were filled with a hybrid resin reinforced

with Portland cement <sup>1</sup> – see Figure 11 for a side view of the reinforced gripping sections.

## 5. Results and discussion

### 5.1. Modal analysis

Comparison of modal analysis results is made by computing the MAC between the experimental and the FE results. Indeed, MAC values are a useful indicator of the similarity between test and analysis mode shapes. It is defined as a scalar constant relating the degree of consistency (linearity) between one modal and another reference modal vector as follows:

$$\text{MAC}(A, X) = \frac{|\{\psi_X\}^T \{\psi_A\}|^2}{(\{\psi_X\}^T \{\psi_X\}) \cdot (\{\psi_A\}^T \{\psi_A\})} \quad (6)$$

where  $\psi_X$  and  $\psi_A$  are the experimental and FE-based eigenvectors respectively. The value of the MAC is proportional to the correlation of the two mode shapes with a maximum of 1.

Moreover, in order to check the accuracy of the FE models, a comparison of the eigenfrequencies is performed. In the following, results for the four tested panels are shown and compared with FE models built assuming, in the analytical formulation, either the sinusoidal shape – usually referred to as *theoretical* and abbreviated in “*th.*” – or the real corrugated profile – usually abbreviated in “*real*”.

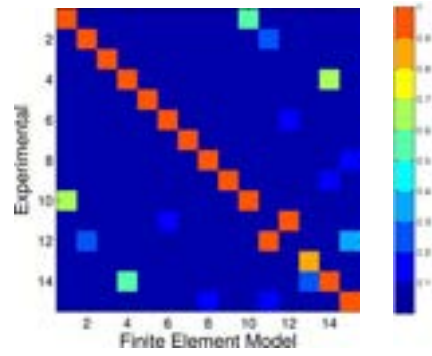
#### 5.1.1. 05\_02\_05 H6

MAC comparison for this first panel is shown in Figure 12. It is important noting that the FE model which implements the general formulation for real corrugated profiles shows a better behaviour than the sinusoidal corrugated model. Indeed, the mode switch between modes 11 and 12, which can be seen for the sinusoidal shape in Figure 12a, is not present in the comparison with the real corrugated core panel, in Figure 12b.

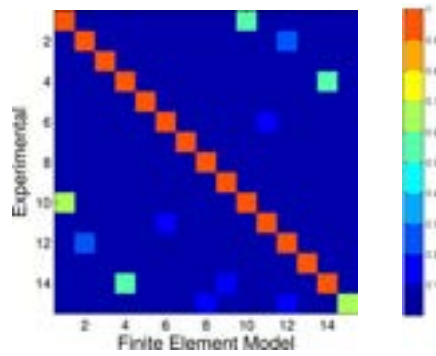
Even more relevant to prove the importance of accurately modelling the core profile is the comparison of the eigenfrequencies. In Table 4, the experimentally derived values are compared to FE model results. It is important noting that frequencies are listed and sorted according to the experimentally

---

<sup>1</sup>Fisher. T-Bond Fixing – [www.fischeritalia.it/prodotti/t-bond](http://www.fischeritalia.it/prodotti/t-bond)



(a)



(b)

Figure 12: 05\_02\_05 H6 panel. MAC comparison between experimental data and FE models with: (a) Theoretical core, (b) Real core.

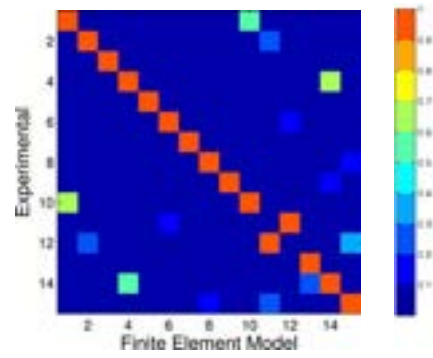
Mode No.	Exp. [Hz]	FE th. [Hz]	Th. err. [%]	FE real [Hz]	Real err. [%]
1	91.4	99.4	+8.69	97.2	+6.37
2	121.8	124.4	+2.08	123.5	+1.32
3	212.2	222.2	+4.75	215.2	+1.42
4	219.4	235.4	+7.28	227.9	+3.87
5	269.7	287.0	+6.44	277.7	+2.96
6	349.8	362.1	+3.52	357.9	+2.30
7	426.5	453.3	+6.29	439.0	+2.95
8	434.0	471.8	+8.69	448.3	+3.29
9	542.3	586.8	+8.21	539.3	-0.54
10	600.1	655.7	+9.26	602.7	+0.43
11	658.7	721.3	+9.50	678.3	+2.97
12	673.2	695.9	+3.37	690.0	+2.50
13	728.4	777.0	+6.66	742.5	+1.93
14	773.6	849.5	+9.82	789.6	+2.08
15	957.6	1047.3	+9.37	948.3	-0.97

Table 4: Comparison of eigenfrequencies for the 05\_02\_05 H6 panel.

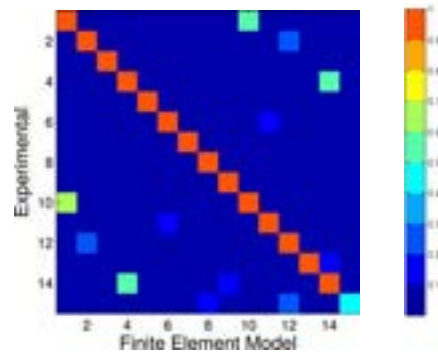
determined values. The FE model with the real shape homogenized core shows an evident greater accuracy than the sinusoidal one. To quantify this difference, a relative error is reported in percentage in the same table, taking the experimental data as reference. Nevertheless, to have an estimation of the overall accuracy for the analyzed modes, the average of the absolute values of such errors is computed. The model with supposed sinusoidal core has mean absolute error of about 6.93%, while for the model with real shaped corrugations this value is 2.39%.

#### 5.1.2. 08\_02\_05 H6

The same procedure was also used for the second panel. The resulting MAC comparison is shown in Figure 13. Also in this case a better agreement is found between the experimental data and real corrugated model results. The same mode inversion is visible in the sinusoidal case, Figure 13a, and avoided in the real corrugation case, Figure 13b. Indeed, this panel has a dynamic behaviour quite similar to the previous panel (05\_02\_05 H6), as it can be seen comparing modal frequencies in Table 5 with the previous Table 4. Nevertheless, FE models for this panel better predict the modal frequencies. Indeed, computing the average absolute error as done before,



(a)



(b)

Figure 13: 08\_02\_05 H6 panel. MAC comparison between experimental data and FE models with: (a) Theoretical core, (b) Real core.

Mode No.	Exp. [Hz]	FE th. [Hz]	Th. err. [%]	FE real [Hz]	Real err. [%]
1	90.5	95.7	+5.78	94.5	+4.48
2	118.6	119.5	+0.73	119.7	+0.86
3	209.1	214.0	+2.37	209.1	-0.01
4	216.1	226.4	+4.78	221.1	+2.30
5	265.5	276.2	+4.04	269.5	+1.49
6	342.6	347.9	+1.55	346.8	+1.22
7	419.7	435.5	+3.78	425.3	+1.34
8	428.1	453.8	+6.01	434.6	+1.52
9	535.8	564.5	+5.36	522.1	-2.56
10	593.0	630.6	+6.34	583.3	-1.64
11	650.8	693.2	+6.52	656.5	+0.88
12	655.7	668.0	+1.88	668.1	+1.90
13	714.2	746.1	+4.47	718.4	+0.58
14	763.1	816.4	+6.98	763.8	+0.10
15	942.4	1005.6	+6.71	914.8	-2.93

Table 5: Comparison of eigenfrequencies for the 08\_02\_05 H6 panel.

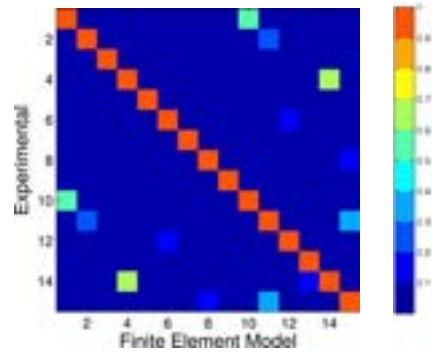
the sinusoidal model leads to a value of 4.48% against the 1.59% of the real core model.

#### 5.1.3. 10\_03\_10 H6

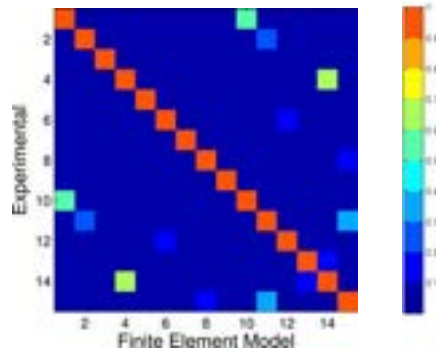
The third panel has thicker faces than the previous ones, 1 mm for each skin, being equal the total thickness of the panel. This implies that the core has a weaker influence on the overall behaviour, even though it is made of a thicker lamina than previous cases, i.e. 0.3 mm. Therefore, the difference between supposed sinusoidal and real shape is less noticeable. This consideration is evident looking both at the MAC comparison in Figure 14 and at the frequency comparison in Table 6. From Figure 14, almost no difference can be seen in the two graphs and the improvement in the average error in Table 6 is reduced: 0.73% for the real shaped model against the 1.58% of the sinusoidal cored model.

#### 5.1.4. 10\_03\_10 H11.5

The fourth and last panel tested is the most challenging. Indeed, even though the lamina thicknesses are the same (1 mm for the faces and 0.3 mm for the corrugated core), the height of the core layer is much bigger, i.e. 9.5



(a)



(b)

Figure 14: 10\_03\_10 H6 panel. MAC comparison between experimental data and FE models with: (a) Theoretical core, (b) Real core.

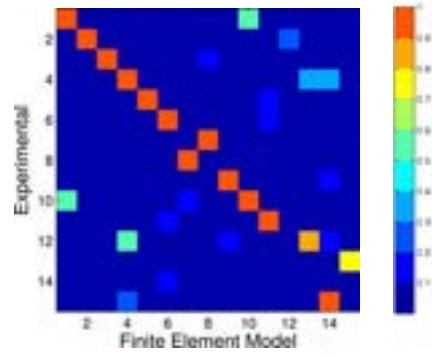
Mode No.	Exp. [Hz]	FE th. [Hz]	Th. err. [%]	FE real [Hz]	Real err. [%]
1	92.0	93.9	+2.02	93.5	+1.59
2	116.7	115.6	−0.93	115.7	−0.86
3	210.7	211.4	+0.34	210.2	−0.27
4	219.3	222.6	+1.50	220.8	+0.68
5	268.6	272.0	+1.26	270.2	+0.62
6	337.9	338.0	+0.03	337.7	−0.06
7	422.2	427.3	+1.19	423.9	+0.39
8	439.0	449.9	+2.48	444.3	+1.20
9	560.2	567.1	+1.23	555.0	−0.92
10	621.6	633.4	+1.89	619.7	−0.31
11	644.8	647.7	+0.45	648.0	+0.50
12	670.5	689.4	+2.82	678.0	+1.12
13	720.9	732.8	+1.65	726.7	+0.80
14	796.3	819.3	+2.90	800.9	+0.58
15	973.6	1002.6	+2.98	983.3	+0.99

Table 6: Comparison of eigenfrequencies for the 10\_03\_10 H6 panel.

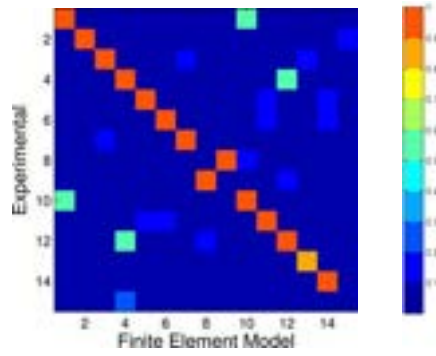
Mode No.	Exp. [Hz]	FE th. [Hz]	Th. err. [%]	FE real [Hz]	Real err. [%]
1	175.7	185.0	+5.29	177.5	+1.04
2	239.0	237.9	−0.47	237.7	−0.55
3	377.6	407.5	+7.91	365.3	−3.26
4	402.0	428.1	+6.50	397.4	−1.15
5	476.0	519.2	+9.08	464.6	−2.38
6	669.3	680.5	+1.68	674.5	+0.78
7	727.9	820.0	+12.66	708.2	−2.69
8	770.9	818.2	+6.14	763.2	−0.99
9	799.9	962.9	+20.38	738.7	−7.66
10	897.4	1071.6	+19.41	843.3	−6.03
11	1078.9	1223.2	+13.37	1057.1	−2.02
12	1116.2	1327.0	+18.88	1062.1	−4.84
13	1227.3	1608.3	+31.04	1116.9	−9.00
14	1318.4	1688.4	+28.06	1202.4	−8.80
15	1342.5	1432.6	+6.71	1358.0	+1.16

Table 7: Comparison of eigenfrequencies for the 10\_03\_10 H11.5 panel.





(a)



(b)

Figure 15: 10\_03\_10 H11.5 panel. MAC comparison between experimental data and FE models with: (a) Theoretical core, (b) Real core.

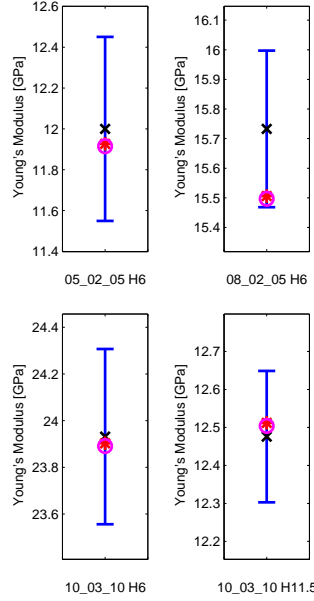


Figure 16: Comparison between experimental Young's modulus and analytical values in the  $x$ -direction.

mm, leading to a very weak core. According to the same comparison of MAC values, Figure 15, it is now clear that both the sinusoidal and the real corrugated models are less accurate in predicting the dynamic behaviour of the real panel if compared with previous thinner structures. Nevertheless, the improvement in the accuracy that can be achieved with a proper modelling of the core profile can be seen comparing MAC values for the supposed sinusoidal shape, Figure 15a, with the values from the real corrugated model, Figure 15b. This consideration is also confirmed by the eigenfrequency comparison, Table 7, where a general bigger error in predicting the values can be seen, especially at higher frequency. Nevertheless, the average error for the real shaped model is 3.49%, drastically reducing the 12.51% of the sinusoidal core model. Please note that, to compute relative differences for the 15th experimental mode, the 16th mode of the FE models is used, since a mode inversion is present between these two modes. It is finally important noting that the thicker the panel, the greater the error is in modelling it as a bidimensional component.

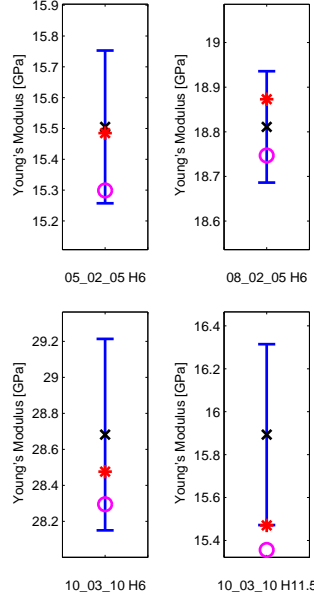


Figure 17: Comparison between experimental Young's modulus and analytical values in the  $y$ -direction.

### 5.2. Tensile testing

Comparison of results is shown in Figures 16 and 17 by plotting the average experimental Young's modulus (black cross in the figures) with the related confidence interval (blue lines) and overlapping the analytical result supposing a perfectly sinusoidal core (magenta circle) and the analytical result computed considering the real shape of the corrugations (red asterisk). In Figure 16, the comparison is shown for the four panels in the  $x$ -direction, while in Figure 17, Young's modulus in the  $y$ -direction is considered. Even though the confidence interval was computed on small data groups – only 5 specimens for each kind of panel in each direction – these graphs are useful for a first understanding. Nevertheless, it is worth noting that experimental values are rather scattered, as it can be seen looking at Table 8 where experimental results are summarized and an estimation of the variability is given by means of the standard deviation parameter.

As it can be seen from the two figures, a very good agreement is found between experimental and analytical values. This observation is validated by computing the percentage errors between analytical and average experimental results, assuming the latter as reference, which are listed in Table 9. It is

Panel type and direction	Min. value [GPa]	Ave. value [GPa]	Max. value [GPa]	Std. Dev. [MPa]
05_02_05 H6(x)	11.45	12.00	12.42	324.69
08_02_05 H6(x)	15.51	15.73	16.07	190.36
10_03_10 H6(x)	23.59	23.93	24.30	270.66
10_03_10 H11.5(x)	12.32	12.48	12.70	124.54
05_02_05 H6(y)	15.19	15.89	16.38	178.56
08_02_05 H6(y)	18.67	18.81	18.92	89.94
10_03_10 H6(y)	28.15	28.68	29.20	383.06
10_03_10 H11.5(y)	15.53	15.89	16.38	303.79

Table 8: Summary of measured Young’s moduli.

Panel type (direction)	Exp. ave. [GPa]	Th. core [GPa]	Th. core Err. [%]	Real core [GPa]	Real core Err. [%]	Skins [GPa]
05_02_05 H6(x)	12.00	11.92	−0.71	11.93	−0.61	11.60
05_02_05 H6(y)	15.51	15.30	−1.33	15.49	−0.13	11.60
08_02_05 H6(x)	15.73	15.50	−1.50	15.51	−1.44	15.17
08_02_05 H6(y)	18.81	18.75	−0.34	18.87	+0.33	15.17
10_03_10 H6(x)	23.93	23.89	−0.17	23.90	−0.12	23.43
10_03_10 H6(y)	28.68	28.30	−1.35	28.48	−0.72	23.43
10_03_10 H11.5(x)	12.48	12.50	+0.23	12.51	+0.29	12.23
10_03_10 H11.5(y)	15.89	15.36	−3.38	15.47	−2.66	12.23

Table 9: Comparison equivalent Young’s moduli for the complete tested panels.

worth noting that, as already visible in Figures 16 and 17, a slightly greater accuracy is provided by assuming in the analytical formulation the real shape of the corrugation (“Real core” in Table 9) respect to a theoretical sinusoidal core (“Th. core” in Table 9). In particular, in one case, the 10\_03\_10 H11.5 panel, the analytical Young’s modulus in the *y-direction* supposing sinusoidal shape is out of the confidence interval determined by measurements. Nevertheless, the relative errors are usually comparable. This can be attributed to the smaller influence the real corrugation has on the equivalent Young’s moduli of the core layer, respect to the influence on the shear moduli, which were the main drivers of the differences in the modal analysis. For a quantitative idea, in the last column of Table 2, the contribution of the skins is reported. Moreover, the difference between the two corrugations is greater in the *y-direction*. This is mainly due to the fact that in the *y-direction*, the Young’s modulus of the complete panel is more contributed by the equivalent core modulus than in the *x-direction*. Indeed, although the main contribution is that of the skins, the core has a particular relevance in the *y-direction*, even though it cannot be disregarded even in the *x-direction*.

Finally, errors in the *y-direction* are generally higher than in the *x-direction*. One reason for this behaviour is the influence of the glue, which in that direction gives a non-negligible structural contribution.

## 6. Conclusions

The present paper has shown the results of an experimental campaign set up on available aluminium sandwich panels with sinusoidally corrugated core.

The first observation on the core of the available panels has shown a corrugation shape which differs from the supposed theoretical sinusoid. The effect of this difference has been investigated and it has been shown that the real corrugation implies a reduction of several parameters with a particular influence on one transverse shear modulus, which is decreased by around 60%. Therefore, in the following comparison with experimental results, both the sinusoidal shape and the real corrugation are assessed.

The first test consists in a modal analysis of the four different available panel configurations. The first 15 modes have been extracted and compared with results from FE models where the complex shaped core was represented as an equivalent homogeneous layer with results from [1] and extended according to Section 2. Results have shown the model built with the analytical

formulation to be very representative of measurement data. Moreover, modelling the equivalent core layer starting from a reproduction of the real core profile allows drastically improving the accuracy of the model with supposed perfectly sinusoidal corrugation. Nevertheless, some differences in the modal behaviour were observed between the tested panels and the FE homogenized models. These differences can be partially attributed to the hypothesis of perfect bonding between equivalent core layer and panel skins. This assumption, implicitly made when using the PCOMP property in Nastran, leads to a smeared model which is only an approximation. Finally, neglecting of the through thickness effects, such as thickness reduction of the core layer, which are not represented by the FE model, could introduce errors. Nevertheless, other sources of error should be investigated, e.g. the influence of the glue on the overall dynamic characteristics.

The second test is a tensile testing on the complete panels in the two main directions of the panel plane. In both directions, the analytical formulation has shown a good accuracy in predicting the mechanical properties of the panel. In general the accuracy of the analytical formulation considering the real shaped core is higher than that of the theoretical sinusoidal corrugation. Nevertheless, the difference between the two core shapes is now less evident, compared to the previous modal analysis, since it results in a smaller difference in the Young's moduli of the complete panels. This is due both to the smaller influence of the shape on the core Young's moduli, compared to shear moduli, and to the smaller influence of the equivalent core to the total panel behaviour. Moreover, the error in the *y-direction* is bigger than that in the *x-direction*. The reason behind this phenomenon has probably to be found in the effect of the presence of the glue.

Further development of the present experimental analysis would require more specimens to be tested in the tensile testing, in order to be able to statistically analyze data and achieve more significant results. Indeed, the variability of available tensile data was sometimes too high to have a good comparison term for the analytical modelling. Moreover, the specimens for tensile tests are obtained, for each configuration, from only one panel, which is the only one available and already used for the experimental modal analysis. Therefore, it could be interesting to investigate the variability of the mechanical and modal characteristics among different panels. Finally, the presence of the glue, both on the static and modal behaviour should be investigated more deeply, since it is likely to influence the global properties.

## References

- [1] G. Bartolozzi, N. Baldanzini, M. Pierini, Equivalent properties for corrugated cores of sandwich structures: A general analytical method, *Composite Structures* 108 (2014) 736–746, ISSN 02638223, doi:10.1016/j.compstruct.2013.10.012.
- [2] L. A. Carlsson, T. Nordstrand, B. O. Westerlind, On the Elastic Stiffnesses of Corrugated Core Sandwich, *Journal of Sandwich Structures and Materials* 3 (4) (2001) 253–267, ISSN 10996362, doi:10.1106/BKJF-N2TF-AQ97-H72R.
- [3] A. C. Gilchrist, J. C. Suhling, T. J. Urbanik, Nonlinear finite element modeling of corrugated board, *American Society of Mechanical Engineers, Applied Mechanics Division, AMD* 231 (1999) 101–106.
- [4] Z. Aboura, N. Talbi, S. Allaoui, M. L. Benzeggagh, Elastic behavior of corrugated cardboard: experiments and modeling, *Composite Structures* 63 (1) (2004) 53–62, ISSN 02638223, doi:10.1016/S0263-8223(03)00131-4.
- [5] S. Allaoui, Z. Aboura, M. L. Benzeggagh, Effects of the environmental conditions on the mechanical behaviour of the corrugated cardboard, *Composites Science and Technology* 69 (1) (2009) 104–110, ISSN 02663538, doi:10.1016/j.compscitech.2007.10.058.
- [6] S. Allaoui, Z. Aboura, M. L. Benzeggagh, Phenomena governing uni-axial tensile behaviour of paperboard and corrugated cardboard, *Composite Structures* 87 (1) (2009) 80–92, ISSN 02638223, doi:10.1016/j.compstruct.2008.01.001.
- [7] P. Patel, T. Nordstrand, L. A. Carlssonb, Local buckling and collapse of corrugated board under biaxial stress, *Composite Structures* 39 (1) (1997) 93–110.
- [8] T. Nordstrand, Analysis and testing of corrugated board panels into the post-buckling regime, *Composite Structures* 63 (2) (2004) 189–199, ISSN 02638223, doi:10.1016/S0263-8223(03)00155-7.

- [9] F. Côté, V. S. Deshpande, N. A. Fleck, A. G. Evans, The compressive and shear responses of corrugated and diamond lattice materials, *International Journal of Solids and Structures* 43 (20) (2006) 6220–6242, ISSN 00207683, doi:10.1016/j.ijsolstr.2005.07.045.
- [10] L. Torre, J. M. Kenny, Impact testing and simulation of composite sandwich structures for civil transportation, *Composite Structures* 50 (3) (2000) 257–267, ISSN 02638223, doi:10.1016/S0263-8223(00)00101-X.
- [11] E. M. Knox, M. J. Cowling, I. E. Winkle, Adhesively bonded steel corrugated core sandwich construction for marine applications, *Marine Structures* 11 (4-5) (1998) 185–204, ISSN 09518339, doi:10.1016/S0951-8339(98)40651-8.
- [12] K. Magnucki, P. Jasion, M. Krus, P. Kuligowski, L. Wittenbeck, Strength and buckling of sandwich beams with corrugated core, *Journal of Theoretical and Applied Mechanics* 51 (1) (2013) 15–24.
- [13] C. A. Castigliano, *Intorno ai sistemi elastici*, Dissertation, Politecnico di Torino, IT, 1873.
- [14] G. Bartolozzi, M. Pierini, U. Orrenius, N. Baldanzini, An equivalent material formulation for sinusoidal corrugated cores of structural sandwich panels, *Composite Structures* 100 (2013) 173–185, ISSN 02638223, doi:10.1016/j.compstruct.2012.12.042.
- [15] R. J. Allemang, The Modal Assurance Criterion – Twenty Years of Use and Abuse, *Sound and Vibration* 1 (2003) 14–21.
- [16] MSC.Software, MD Nastran 2010r1, Quick reference guide, 2010.
- [17] American Society for Testing and Materials, ASTM C297 - Standard Test Method for Flatwise Tensile Strength of Sandwich Construction, 2004.
- [18] American Society for Testing and Materials, ASTM C365 - Standard Test Method for Flatwise Compressive Properties of Sandwich Cores, 2003.
- [19] American Society for Testing and Materials, ASTM C273 - Standard Test Method for Shear Properties of Sandwich Core Materials, 2000.



- [20] T. Yokozeki, S. I. Takeda, T. Ogasawara, T. Ishikawa, Mechanical properties of corrugated composites for candidate materials of flexible wing structures, *Composites Part A: Applied Science and Manufacturing* 37 (10) (2006) 1578–1586, ISSN 1359835X, doi: 10.1016/j.compositesa.2005.10.015.
- [21] American Society for Testing and Materials, ASTM E8 - Standard Test Methods for Tension Testing of Metallic Materials, 2008.
- [22] American Society for Testing and Materials, ASTM D3039 - Standard Test Method for Tensile Properties of Polymer Matrix Composite Materials, 2008.